AIAA SPACE Forum
4-7 August 2014, San Diego, CA
AIAA SPACE 2014 Conference and Exposition

10.2514/6.2014-4344

Check for updates

Using VASIMR® for the Proposed Europa Mission

Edgar A. Bering, III[1], Matthew Giambusso[2],
University of Houston, Department of Physics, Houston, TX 77204, USA

Mark Carter[3], Andrew Ilin[4], Chris S. Olsen[5], Jared P. Squire[6], Franklin R. Chang Díaz[7]
Ad Astra Rocket Company, Webster, TX 77598, USA

and

Benjamin W. Longmier[8]
University of Michigan, Department of Aerospace Engineering, Ann Arbor, Michigan, 48109, USA

Downloaded by University of Michigan - Duderstadt Center on December 13, 2017 | http://arc.aiaa.org | DOI: 10.2514/6.2014-4344

We explore the capability of a VASIMR® reusable probe "catapult" concept to send a 4000-5000 kg spacecraft to Jupiter on a Hohmann-like transfer orbit, arriving in just 36 months elapsed time. The VASIMR® performs a slingshot pass close to the Sun and uses the high level of available solar energy to produce a sustained burst of high thrust. Enough kinetic energy is provided to the probe to reach Jupiter orbit within 0.7-1.4 AU. The Catapult release the probe with enough speed to reach Jupiter in three years, and returns to Earth for another mission. This study identifies the important parameters in the probe ejector operation (power level, propellant mass, payload release point, distance of closest approach to the Sun), and scan these parameters to understand and optimize the capabilities of the proposed system. We assume that the Catapult and its payload begin at the Earth's sphere of influence (SOI), and are coasting in the Earth's orbit about the Sun. The VASIMR® engine's power rating must match the peak power available when the spacecraft is closest to the Sun. The solar array is assumed to be a planar array rather than a concentrator since it will have to operate near the Sun, where a concentrator would overheat photovoltaic cells. The feasibility of not releasing the payload and using the VASIMR® to provide thrust for the duration of the transfer orbit will also be examined. In this scenario, the VASIMR® RF generators could serve double duty as radar RF sources.

Nomenclature

η_A	=	ICH coupler efficiency
η_b	=	ion coupling efficiency
f	=	frequency
f_{ci}	=	ion cyclotron frequency
F	=	ion velocity phase space distribution function
Γ_i	=	total ion flux
I_{sp}	=	specific impulse

[1] Professor, Physics and ECE, 617 Science & Research I /PHYS 5005, Associate Fellow.
[2] Graduate Student, Physics, 617 Science & Research I/PHYS 5005
[3] Director of Technology, Ad Astra Rocket Company, 141 W. Bay Area Blvd, Member.
[4] Computational Research Lead, Ad Astra Rocket Company, 141 W. Bay Area Blvd, Member.
[5] Senior Research Scientist, Ad Astra Rocket Company, 141 W. Bay Area Blvd., Member
[6] Vice President of Research, Ad Astra Rocket Company, 141 W. Bay Area Blvd., Member.
[7] Chief Executive Officer, Ad Astra Rocket Company, 141 W. Bay Area Blvd., Associate Fellow.
[8] Assistant Professor, Department of Aerospace Engineering, University of Michigan, longmier@umich.edu

Copyright © 2014 by University of Houston.
Published by the American Institute of Aeronautics and Astronautics, Inc., with permission.

L_A = inductance of the ICH coupler
L_M = inductance of the ICH coupler matching network
m_{doti} = mass flow rate
P_{plasma} = ICH RF power broadcast into plasma
P_{ion} = ICH RF power coupled into ions
P_{ICH} = ICH RF power into coupler
Q_c = quality factor of the ICH coupler circuit
R_c = resistance of the ICH coupler circuit
R_p = plasma loading of the ICH coupler
Θ = pitch angle
v_{ICRF} = exhaust plasma flow velocity with ICH on
$v_{helicon}$ = exhaust plasma flow velocity with helicon only
$VSWR_{plasma}$ = voltage standing wave ratio of the ICH coupler, with plasma present
$VSWR_{vacuum}$ = voltage standing wave ratio of the ICH coupler, with no plasma present
W_{ICH} = mean ion energy increase owing to ICH

ω = angular frequency

Downloaded by University of Michigan - Duderstadt Center on December 13, 2017 | http://arc.aiaa.org | DOI: 10.2514/6.2014-4344

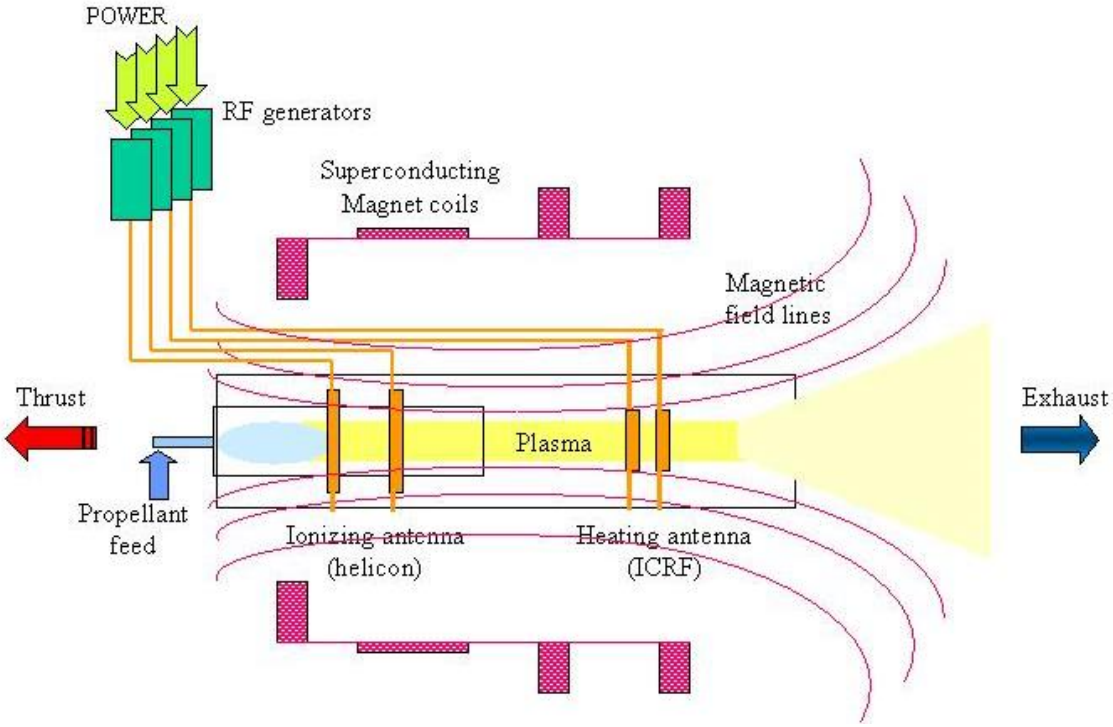

Figure 1. Cartoon block diagram of the VASIMR™ system, illustrating the basic physics.

I. Introduction

THE exploration of the solar system will be one of the defining scientific tasks of the new century. One of the obvious challenges faced by this enterprise is the scale size of the system under study, 10^{11} - 10^{14} m. Over distances on this scale and given the performance of present day rockets, the mission designer is faced with the choice of accepting multi-year or even decadal mission time lines, paying for enormous investment in rocket propellant compared to useful payload, or finding a way to improve the performance of today's chemical rockets. For human space flight beyond Earth's orbit, medical, psychological, and logistic considerations all dictate that drastic thruster improvement is the only choice that can be made. Even for robotic missions beyond Mars, mission time lines of years can be prohibitive obstacles to success, meaning that improvements in deep space sustainer

engines are of importance to all phases of solar system exploration[1]. The need for high performance interplanetary transfer vehicles has been underlined by the recent discovery of geyser activity on the Jovian moon, Europa. The scientific interest provoked by these observations has prompted initial mission design and planning efforts aimed at sending an orbiter to investigate these sightings. This paper will explore the role that the VASIMR® engine could play in facilitating and enhancing such a mission.

Better thruster performance can best be achieved by using an external energy source to accelerate or heat the propellant[2,3]. High-power electric propulsion thrusters can reduce propellant mass for heavy-payload orbit-raising missions and cargo missions to the Moon and near Earth asteroids and can reduce the trip time of robotic and piloted planetary missions.[1,4,5,6] The Variable Specific Impulse Magnetoplasma Rocket (VASIMR®) VX-200 engine is an electric propulsion system capable of processing power densities on the order of 6 MW/m^2 with a high specific impulse and an inherent capability to vary the thrust and specific impulse at a constant power. The potential for long lifetime is due primarily to the radial magnetic confinement of both ions and electrons in a quasi-neutral flowing plasma stream, which acts to significantly reduce the plasma impingement on the walls of the rocket core. High temperature ceramic plasma-facing surfaces handle the thermal radiation, the principal heat transfer mechanism from the discharge. The rocket uses an optimized helicon plasma source[7,8] for efficient plasma production in the first stage. This plasma is energized further by an ion cyclotron heating (ICH) RF stage that uses left hand polarized slow mode waves launched from the high field side of the ion cyclotron resonance. Useful thrust is produced as the plasma accelerates in an expanding magnetic field, a process described by conservation of the first adiabatic invariant as the magnetic field strength decreases in the exhaust region of the VASIMR®.[9,10,11] This paper will discuss an experimental investigation of the use of Ion Cyclotron Heating (ICH) to provide an efficient method of electrodeless plasma acceleration in the VASIMR® engine. Particular emphasis in this paper will be placed on investigation of the spatial structure of the exhaust plume and recent advances in system performance.

Research on the VASIMR® engine began in the late 1970's, as a spin-off from investigations on magnetic divertors for fusion technology[12]. A simplified schematic of the engine is shown in Figure 1. The VASIMR® consists of three main sections: a helicon plasma source, an ICH plasma accelerator, and a magnetic nozzle[3,13,14,15,16,17]. Figure 2 shows these three stages integrated with the necessary supporting systems. One key aspect of this concept is its electrode-less design, which makes it suitable for high power density and long component life by reducing plasma erosion and other materials complications. The magnetic field ties the three stages together and, through the magnet assemblies, transmits the exhaust reaction forces that ultimately propel the ship.

The plasma ions are accelerated in the second stage by ion cyclotron resonance heating (ICH), a well-known technique, used extensively in magnetic confinement fusion research[18,19,20,21,22]. Owing to magnetic field limitations on existing superconducting technology, the system presently favors light propellants. However, the helicon, as a stand-alone plasma generator, can efficiently ionize heavier propellants such as argon and xenon.

Downloaded by University of Michigan - Duderstadt Center on December 13, 2017 | http://arc.aiaa.org | DOI: 10.2514/6.2014-4344

Downloaded by University of Michigan - Duderstadt Center on December 13, 2017 | http://arc.aiaa.org | DOI: 10.2514/6.2014-4344

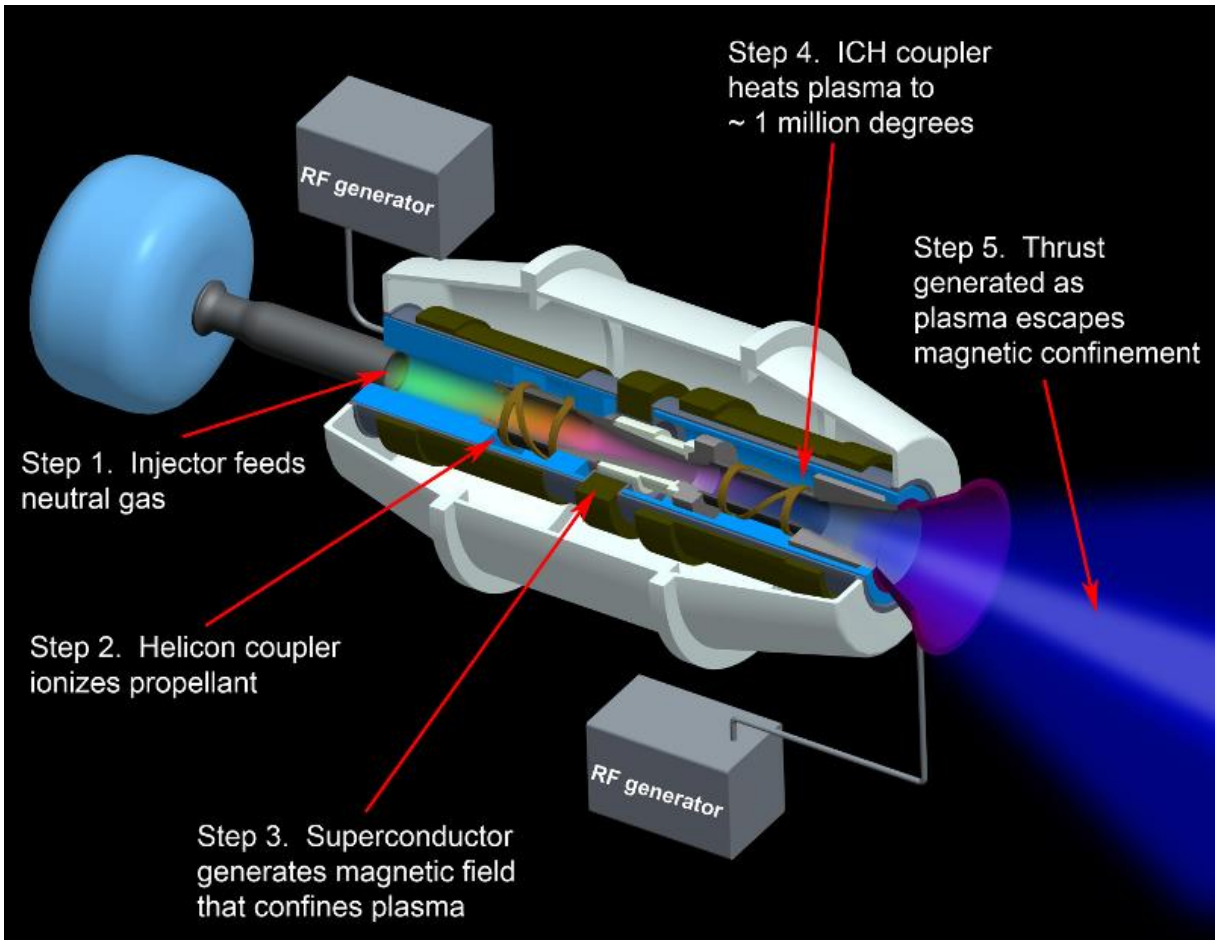

Figure 2. Schematic of the VASIMR® VX-200.

An important consideration involves the rapid absorption of ion cyclotron waves by the high-speed plasma flow. This process differs from the familiar ion cyclotron resonance utilized in tokamak fusion plasmas as the particles in VASIMR® pass through the coupler only once[17,23,24,25]. Sufficient ion cyclotron wave (ICW) absorption has nevertheless been predicted by recent theoretical studies[26], as well as observed and reported in various conferences and symposia.

Elimination of a magnetic bottle, a feature in the original VASIMR® concept, was motivated by theoretical modeling of single-pass absorption of the ion cyclotron wave on a magnetic field gradient[24]. While the cyclotron heating process in the confined plasma of fusion experiments results in approximately thermalized ion energy distributions, the non-linear absorption of energy in the single-pass process results in a boost, or displacement of the ion kinetic energy distribution. The ions are ejected through the magnetic nozzle before thermal relaxation occurs.

Downloaded by University of Michigan - Duderstadt Center on December 13, 2017 | http://arc.aiaa.org | DOI: 10.2514/6.2014-4344

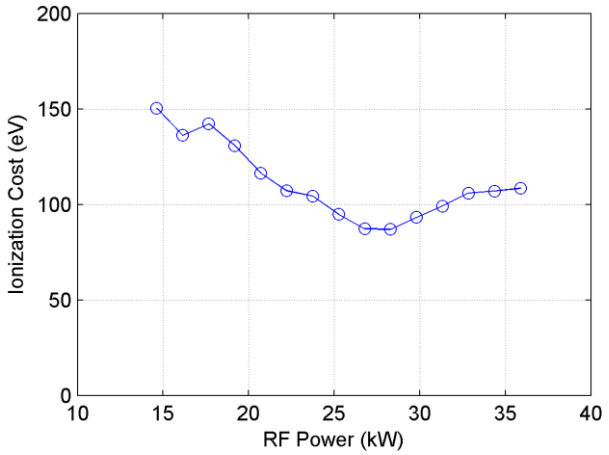

Figure 3. Minimum ionization cost is now 87 ± 9 eV/ion.

Natural processes in the auroral region may also exhibit a related form of single pass ICH. "Ion conic" energetic ion pitch angle distributions are frequently observed in the auroral regions of the Earth's ionosphere and magnetosphere [27,28,29,30,31,32,33]. It is not relevant to list the entire range of models that have been proposed to account for these observations. Many models propose wave-driven transverse ion acceleration followed by adiabatic upwelling of the distribution[34,35 and references therein]. Proposed driver wave modes include current driven electrostatic ion cyclotron (EIC) waves[36,37,38], and electro-magnetic ion cyclotron waves[39,40,41], among others. Other mechanisms proposed include interaction with an oblique double layer or dc potential structure[42,43]. The fact that ion conics are commonly found on auroral field lines suggests that transverse ion acceleration is a ubiquitous process in auroral arcs[35]. Space-borne observations of narrow-band ion-cyclotron waves with unambiguous spectral peaks near the ion cyclotron frequencies are relatively rare[44,45,46,47,48,49,50,51,52]. Most studies have found that the most common wave phenomenon found in association with transverse ion acceleration is broad-band ELF noise[35,53,54,55,56]. All of these authors suggest that current driven EIC waves make up some or all of the broad-band ELF noise, but they are unable to prove it, even when wavelength measurements are available[47,48]. The role of inhomogeneities or shear in reducing the threshold for current-driven EIC instability is suggested as one solution to this problem[48,57]. EMIC waves appear to be associated with transverse ion acceleration ~10% of the time[35,41].

In addition to the extensive body of work on the heating of magnetic confinement fusion plasmas that was superficially cited above, there is a thirty year body of theoretical and laboratory work on transverse ion acceleration by current driven EIC modes[34,36,43,58,59]. All of these experiments have typically used current driven EIC waves, parametric decay of lower hybrid waves, or other mode conversion process to launch the required wave field. Direct injection, which is used in VASIMR®, requires the coupler to have good plasma loading in order to launch the waves with useful efficiency, as discussed below. Since the magnetospheric simulation experiments have aimed at simulating EIC driven heating and VASIMR® uses EMIC waves, these prior results have limited application to the VASIMR®. What has been shown of relevance is that acceleration followed by adiabatic folding is a viable mechanism for producing ion conics[34,59]. However, the field ratios employed were an order of magnitude smaller that used in the VASIMR® studies reported here.

VASIMR® has a transverse ion acceleration stage or booster that uses EMIC waves, followed by adiabatic expansion. Simultaneous ambipolar acceleration is also observed in the VASIMR® exhaust plume that may be interpreted as a large-scale double layer[60]. Thus, VASIMR® results may be of interest to proponents of more than one model of ion conic production.

The VASIMR® engine has three major subsystems, the plasma generator stage, the RF "booster" stage and the nozzle, shown in Figures 1 and 2[16]. Laboratory physics demonstrator experiments (VX-50 and VX-100) were developed and tested first at the NASA Johnson Space Center for several years and more recently at the Ad Astra Rocket Company[61,62]. The details of the engine and its design principles have been previously reported[17,63]. The first stage is a helicon discharge that has been optimized for maximum power efficiency (lowest ionization cost in eV/(electron-ion pair) [64,65,66,67]. The next stage downstream is the heating system. Energy is fed to the system in the form of a circularly polarized rf signal tuned to the ion cyclotron frequency. ICH heating has been chosen because it transfers energy directly and largely to the ions, which maximizes the efficiency of the engine[11,12]. In the present small-scale test version, there is no mirror chamber and the ions make one pass through the ICH coupler. The system also features a two-stage magnetic nozzle, which accelerates the plasma particles by converting their azimuthal energy into directed momentum. The detachment of the plume from the field takes place mainly by the loss of adiabaticity and the rapid increase of the local plasma β, defined as the local ratio of the plasma pressure to the magnetic pressure.

After 10 years of growth and improvement, the VX-50 had achieved all of the physics test goals that could reasonably be obtained. In October, 2006, the VX-50 was decommissioned and disassembled. In its place, the Ad

Astra Rocket Company has built two new machines, the VX-100, which is a laboratory physics demonstrator test bed, and the VX-200, which is a flight-like prototype. The VX-100, a new test bed for the VASIMR® plasma engine, developed by Ad Astra Rocket Company, achieved record performance tests conducted at the company's old

Figure 5. (a) VASIMR® VX-200 prototype.

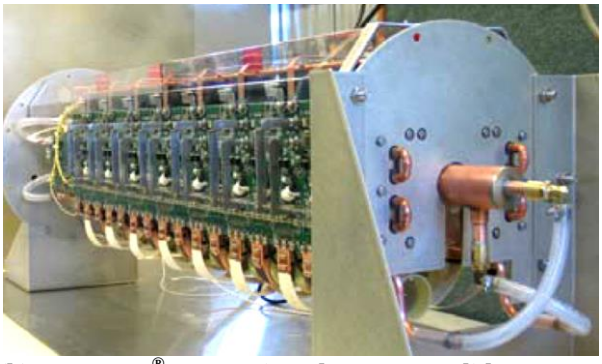

(b) VASIMR® VX-200i and VX-200 solid-state RF amplifier, 1m in length.

Houston laboratory in 2007. The VX-100 test facility, which went into operation in late January of 2007, began to yield reliable experimental data in early February of 2007 and was operated until October 2007.

The VX-200 is a 200kW VASIMR® engine prototype currently in the early stages of the testing phase. The VX-200, completed in May of 2009, is considered by company officials to be the last step before construction of the VF-200 (for VASIMR® flight) series of flight engines planned for space testing in 2014.

The VX-100 and the VX-200 both demonstrated ionization costs below 100 eV/ion (Figure 3). The ionization cost is a measure of the engine's plasma production efficiency with values below 100 being required to ensure efficient operation. Recent tests have focused on the VASIMR® VX-200 ICH second stage.

For the first time, end-to-end testing of the VX-200 engine has been undertaken with an optimum magnetic field and in a vacuum facility with sufficient volume and pumping to permit exhaust plume measurements at low background pressures. Experimental results are presented with the VX-200 engine installed in a 150 m^3 vacuum chamber with an operating pressure below $1x10^{-2}$ Pa ($1x10^{-4}$ Torr), and with exhaust plume diagnostics over a range of 5 m in the axial direction and 1 m in the radial directions. Measurements of plasma flux, RF power, and neutral argon gas flow rate, combined with knowledge of the kinetic energy of the ions leaving the VX-200 engine, are used to determine the ionization cost of the argon plasma. A plasma momentum flux sensor (PMFS) measures the force density as a function of radial and axial position in the exhaust plume. New experimental data on ionization cost, exhaust plume expansion angle, thruster efficiency and total force are presented that characterize the VX-200 engine performance above 100 kW. A semi-empirical model of the thruster efficiency as a function of specific impulse has been developed to fit the experimental data. Recent results at 200 kW DC input power yields a thruster efficiency of 72% at a specific impulse of 5000 s and thrust of 5.8N[11, 68].

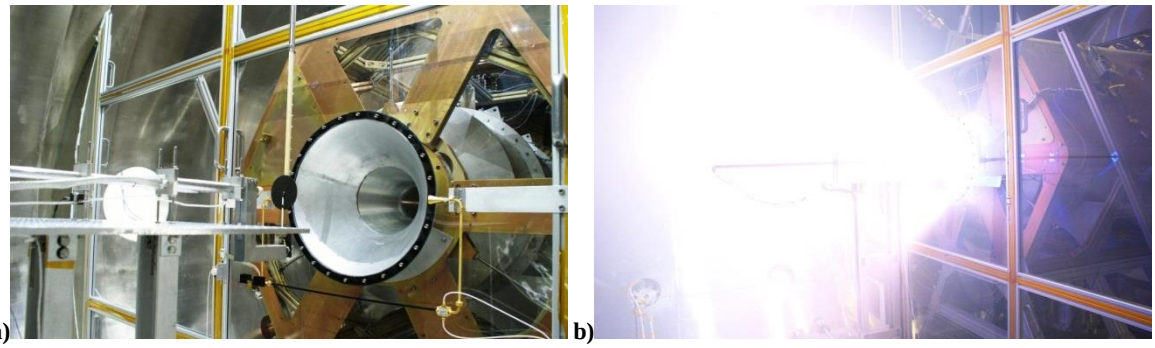

a) **b)**

Fig 4. Photograph of the VX-200 rocket exhaust end facing the diagnostics platform (a), and a high power firing of the VX-200 with immersed plasma diagnostics at closest approach (b).

Downloaded by University of Michigan - Duderstadt Center on December 13, 2017 | http://arc.aiaa.org | DOI: 10.2514/6.2014-4344

II. Experimental Setup

A. The VASIMR® Engine

1. VX-200 and supporting hardware

The VX-200 has a total RF power capability of 200 kW driven by high-efficiency, as high as 98%, solid-state DC-RF generators, as shown in Figure 5b. The VX-200 engine RF generators convert facility DC power to RF power and perform impedance matching between the RF generator output and the rocket core, Fig. 2. The RF generators were custom built by Nautel Ltd., model numbers VX200-1 (helicon generator), and VX200-2 (ICH generator). The VX200-1 RF generator is rated up to 48±1 kW RF with a 91±1% efficiency and a specific mass of 0.85±0.02 kg/kW. The VX200-2 generator is rated up to 172±1 kW RF with a 98±1% efficiency and a specific mass of 0.506±0.003 kg/kW. The generator efficiencies were determined by independent testing performed by Nautel Ltd., which included a direct measurement of input power and calorimetry of the dissipated power in the generator.

The exhaust velocity of the ions increases as the coupled ICH power increases. Coupled RF power is defined as the RF power that is injected by the helicon and/or ICH couplers and is inductively absorbed by the plasma column or radiatively lost by the RF couplers. The coupled RF power is determined by subtracting the power losses in the RF matching network and RF transmission line from the measured RF power at the RF generator output, Fig. 2. Losses in the matching networks and transmissions lines are calculated based on network analyzer measurements of circuit impedance. The efficiency was determined to be 96% for both the helicon and ICH RF circuits.

The helicon plasma source of the VX-200 is driven at 35 kW using 25-150 mg/s of argon gas.. The helicon source internal structure was electrically floating.

The magnetic field in the VX-200 engine is responsible for efficient ion cyclotron coupling of the RF energy to the ions within the quasi-neutral flowing plasma. The applied expanding magnetic field converts perpendicular ion kinetic energy, $E_\perp$, to directed parallel ion kinetic energy, $E_\parallel$, through conservation of the magnetic moment and conservation of the ion's total kinetic energy.[7-9] The location at which 90% of the perpendicular ion energy is converted into parallel ion energy, $E_\parallel/(E_\parallel + E_\perp) = 0.9$, occurs at z = 5 cm, r = 0 cm.

An ambipolar ion acceleration has also been observed[10] and is believed to be the result of the plasma interaction with the magnetic field gradient in the expanding magnetic nozzle of the VX-200 engine, similar to the Boltzman relation but with a varying electron temperature. The ambipolar ion acceleration typically results in an additional directed ion velocity of 5 to 10 km/s, where the energy for this process comes from the electron energy distribution function as a result of electron and ion interaction with a weak electric field in the magnetic nozzle, which ranges in strength from 10 to 20 V/m depending on system parameters.

The data presented in this paper was taken during quasi steady-state operation, up to 30 s in duration. The neutral pressure gradients within the VX-200 engine and the vacuum system equalize within 0.8 s of the initial startup. From 0.8 s through 30 s, the neutral pressure throughout the VX-200 engine and vacuum system are steady-state values. Data for the thruster efficiency calculations was taken during the steady-state portion of the VX-200 operation. The propellant mass flow rate was varied between 50 to 160 mg/s for argon and 100 to 250 mg/s for krypton and was measured by use of a calibrated proportional flow control valve flow controller in addition to a calibrated (NIST traceable) thermal-based mass flow meter that was in-line at the high pressure end of the propellant feed system.

The Ad Astra Rocket Company vacuum chamber is 4.2 m in diameter with a total internal volume of 150 m^3, Figures 6a and 6b, and has four 50,000 l/s cryopanels for a total pumping capability of 200,000 l/s. The vacuum chamber is partitioned into two sections, a rocket section and an exhaust section. The rocket section stays at a space-like vacuum pressure which is lower than the exhaust section while the VX-200 is firing. Also shown in Figure 6b is a 2.5 m by 5 m translation stage that carries a suite of plasma diagnostics for plume characterization. The translation stage uses 2 independent ball screws and is driven by vacuum compatible stepper motors which yield a positional resolution of 0.5 mm. A vertical member mounted to the translation stage holds a mounting table. Each diagnostic is bolted directly to the mounting table for precise alignment and positioning on the translation stage. The red solid line in Figure 6a depicts the full axial range of possible plasma measurements. The red line extends into the VASIMR® VX-200 device, but does not penetrate the helicon source itself, and extends 5 m downstream into the expanding plume region of the vacuum chamber.

Downloaded by University of Michigan - Duderstadt Center on December 13, 2017 | http://arc.aiaa.org | DOI: 10.2514/6.2014-4344

Downloaded by University of Michigan - Duderstadt Center on December 13, 2017 | http://arc.aiaa.org | DOI: 10.2514/6.2014-4344

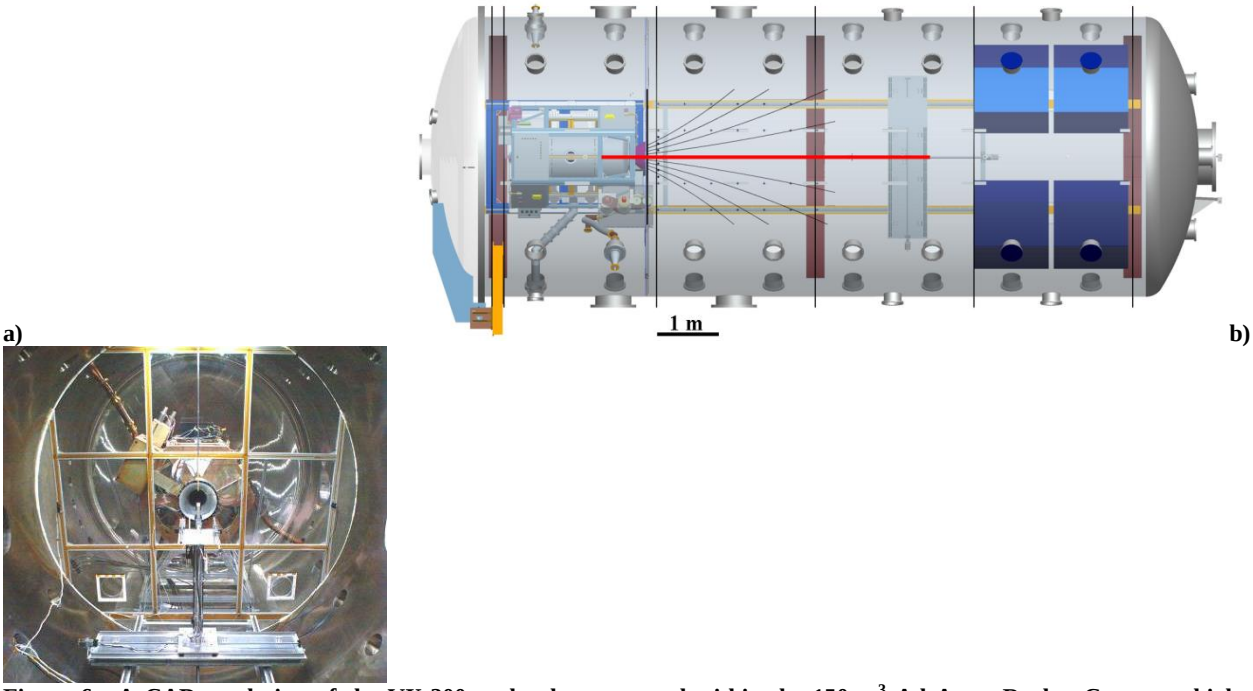

Figure 6. A CAD rendering of the VX-200 rocket bus mounted within the 150 m^3 Ad Astra Rocket Company high vacuum facility with superimposed vacuum magnetic field lines (a), and a photograph of the VX-200 rocket (background) and diagnostics platform (foreground) mounted on a 2 m by 5 m translation stage (b).

III. Efficiency

A. Thruster Performance at 200 kW

For the first time, the total force from the VASIMR VX-200 engine has been measured at the full operating RF power level of 200 kW. The force density within the exhaust plume of the VX-200 engine was measured as a function of the radial and axial position. To determine the total force produced by the VX-200 engine, the force density over one full radius of the exhaust plume, as shown in Figure 7, was integrated using azimuthal symmetry. As the coupled RF power was increased from 28 kW to 200 kW, the total force produced by the VX-200 engine was measured using the PMFS. As shown in Figure 8, the total force increased with increasing ICH coupled RF power as expected.

For the data presented in Figure 7 and Figure 8 the sensor was located at z = 40 cm, where $E_{\parallel}/(E_{\parallel} + E_{\perp}) = 0.98$. The sensor was 9 cm in diameter; small compared to the total exhaust plume diameter of approximately 70 cm. The representative set of force density data for Figure 7 were taken at 14 samples/cm radially from r = 0 cm to r = 40 cm, and 1 sample every 10 cm axially from z = 40 cm to z = 150 cm. The VX-200 engine was operated with 107 mg/s of Ar propellant, a peak magnetic field strength of 2 tesla, a helicon coupled RF power level of 28 kW and an ICH coupled RF power level of 90 kW for the data presented in Figure 7, and an ICH power level range of 0 kW to 172 kW for the data presented in Figure 8. The operating pressure was below 1x10^{-2} Pa (1x10^{-4} Torr) for data taken during 30 s long firings and was below 1x10^{-3} Pa (1x10^{-5} Torr) for the first 800 ms of each firing.

The power scan shown in Figure 8 was accomplished by fixing the helicon power at 30 kW and adding an ICH power ramp up to 170 kW. A gas flow temporal profile was required to achieve the high power ramp while maintaining proper impedance matching. The efficiency data points for less than the highest power were acquired during the power ramp, so are not optimized. These data show that the ICH stage is very effective at accelerating ions with efficiency, defined as the coupled ICH power to ion kinetic energy, of 89%. The acceleration process shows no signs of saturation, as exhibited in Figure 8, since the measured force increases almost linearly until we maximized the available power. Through this scan, the propellant utilization was near 100%, although only the highest power point was optimized for gas flow. The ionization cost is less than or about 100 eV/ion for the helicon alone and we are preparing an effort to study this quantity with ICH power applied. We expect that the lower power points will increase efficiency when we optimize the gas flow for each power setting of the two stages.

Downloaded by University of Michigan - Duderstadt Center on December 13, 2017 | http://arc.aiaa.org | DOI: 10.2514/6.2014-4344

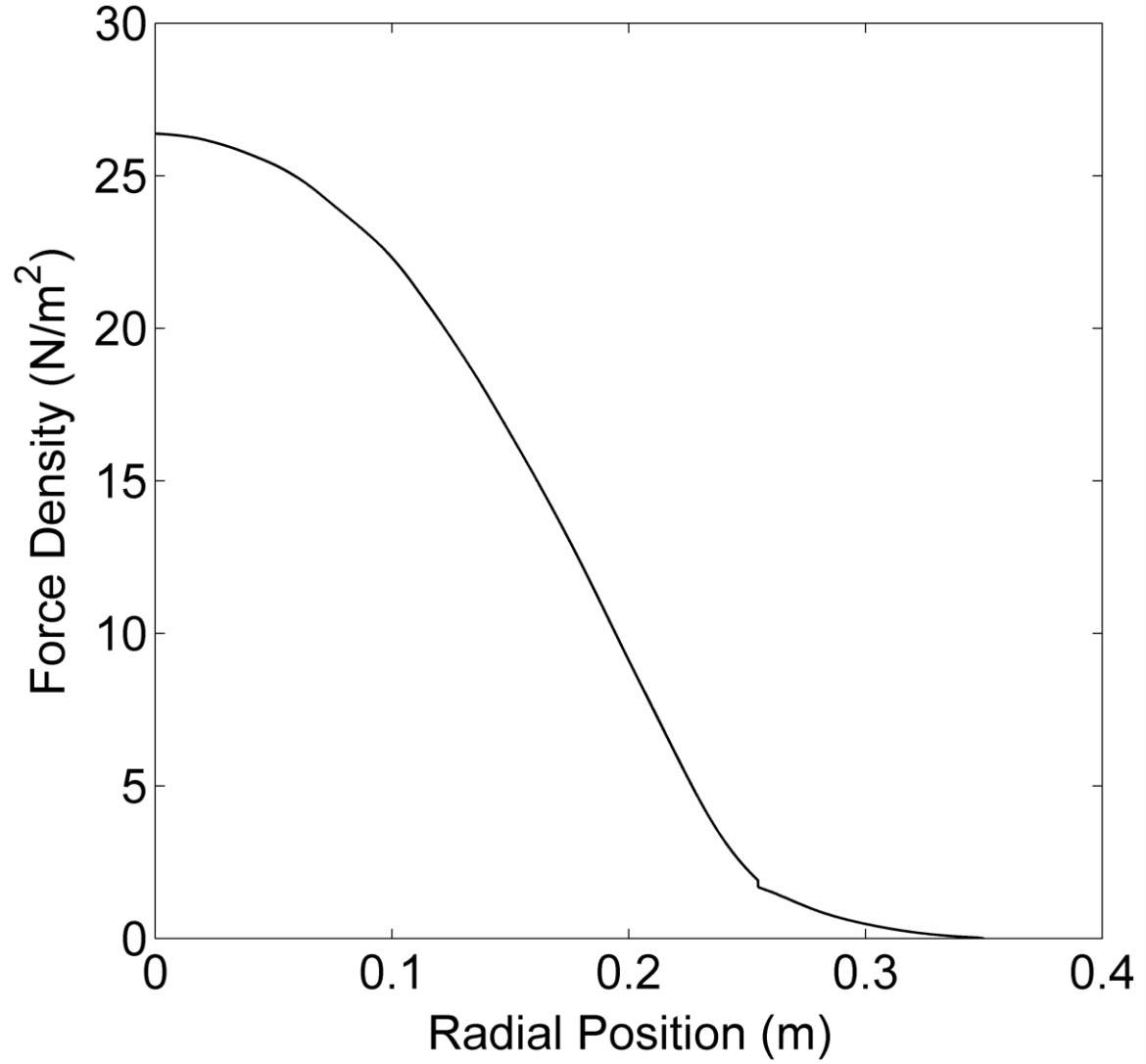

Figure 7. A measured radial profile of the VX-200 engine force density. Error is 7% of the force density value.

Nevertheless, the thruster efficiency with argon gas exceeds 50% for I_{sp} above 3000 seconds and reaches a value of 72 ± 9%, exceeding the extrapolated value near 5000 seconds. The plasma power density at the rocket exit is approximately 5 MW/m^2, where graphite of the force target glows red hot.

No indication of secondary (ArIII) or tertiary (ArIV) ionization states were observed based on optical spectrometer measurements 30 cm downstream of the VX-200 engine exit plane. This implies that the population of ArIII and ArIV ions is at least less than 1% of the ArII population. For the data presented in Fig. 20, the ion-neutral charge exchange mean free path was 10 cm, and for Figures 8 and 9, it was 100 cm.

Measurements of the ionization cost, defined as the ratio of the coupled RF power to the total ion current that is extracted from the system in the exhaust section, were taken during helicon-only operation as a function of both coupled RF power and argon propellant flow rate, from 15 kW to 35 kW and 50 mg/s to 150 mg/s respectively. The lowest ionization cost measurement of 87±9 eV occurred with VX-200 engine settings of 28 kW coupled RF power and 109 mg/s argon flow rate (Figure 3). The ionization cost term, E_i, appears in Eqn 7.

The ion current density and force density were mapped over a large region of the exhaust plume, more than 2 m axially and 1 m radially, with the flat faces of the ion current density probes and the PMFS always in a plane orthogonal to the VX-200 engine axis, i.e. always facing in the direction parallel to the engine axis. This mapping

Downloaded by University of Michigan - Duderstadt Center on December 13, 2017 | http://arc.aiaa.org | DOI: 10.2514/6.2014-4344

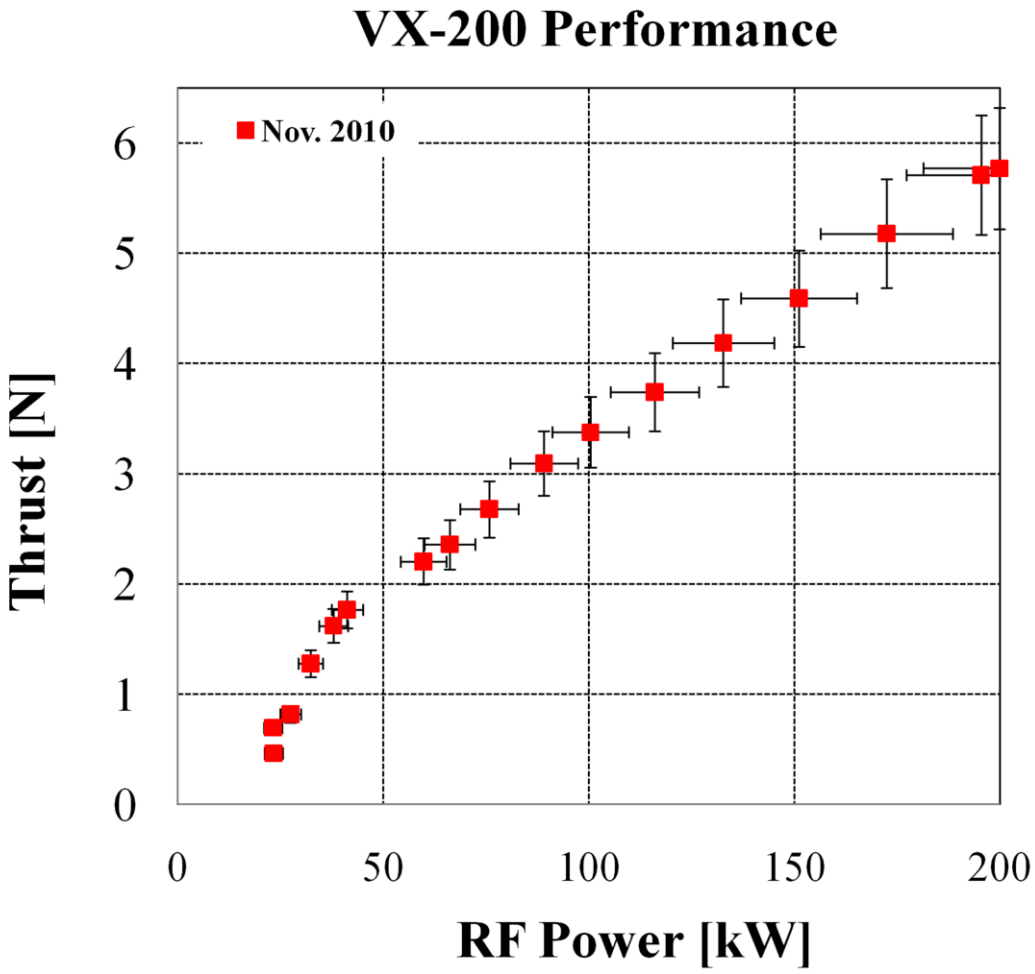

Figure 8. The total force of the VX-200 engine as a function of the measured RF power coupled to the argon plasma.

was performed at a total coupled RF power level of 90 kW and a neutral background pressure of $1x10^{-2}$ Pa ($1x10^{-4}$ Torr). The plasma jet data exhibited a well-defined edge in both ion current density and force density[69] similar to other helicon based devices.[70] Assuming azimuthal symmetry, the conical boundary contour that surrounded 90% of the integrated ion current density and force density was calculated. The angle of that boundary line relative to the VX-200 engine axis, θ, provided an estimate of the exhaust divergence half-angle. The ion current density data yielded a divergence half-angle of 30±2 degrees, while the force density data yielded a divergence half-angle of 24±2 degrees. The half angles were found by radially integrating the ion current density and force density to 90% of the total ion current and total force. These radial maps of ion current density and force density were made between z=40 cm and z=150 cm at 10 cm intervals from the plane of the VX-200 engine exit. The ion flux probe and the force sensor were not rotated such that the ions impacted normal to these surfaces, but were left facing in the direction parallel to the VX-200 engine centerline and translated radially. The conical nozzle correction factor[71] can be used to estimate the fraction of directed momentum to total flow momentum. Here, this correction factor is defined as the nozzle efficiency when expressed as a percentage.

$$\eta_n = \frac{1}{2}(1 + \cos\theta) \tag{3}$$

Downloaded by University of Michigan - Duderstadt Center on December 13, 2017 | http://arc.aiaa.org | DOI: 10.2514/6.2014-4344

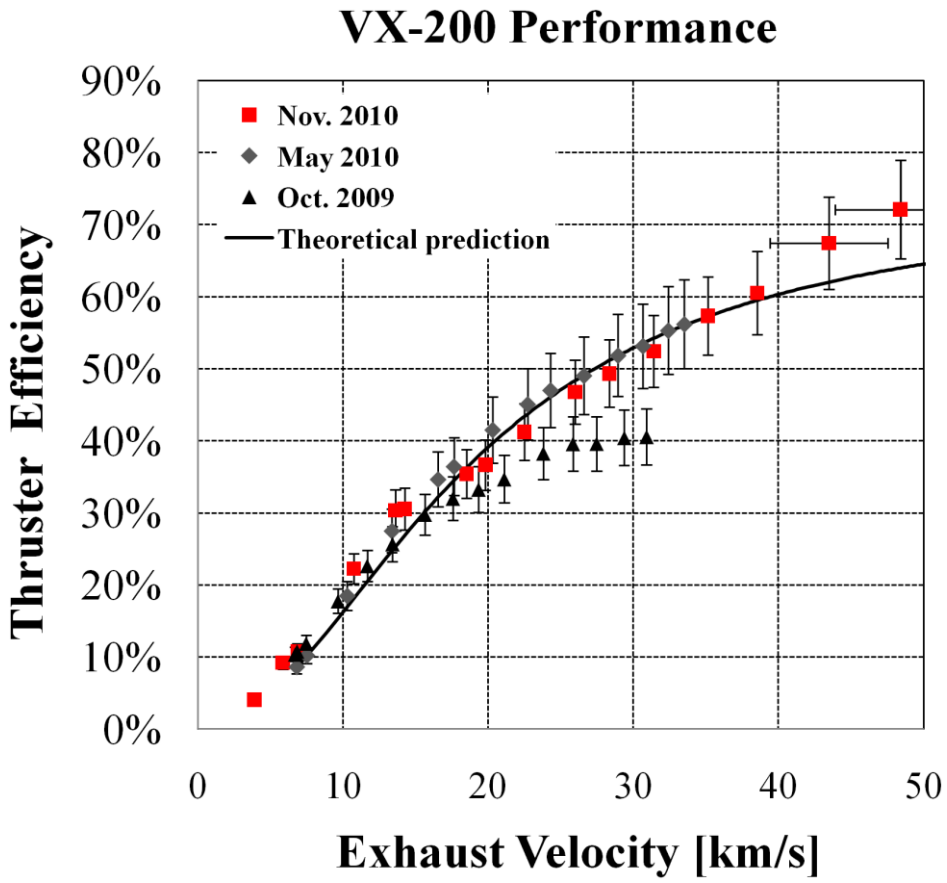

Figure 9. Thruster efficiency vs exhaust velocity (specific impulse x 10). Results are shown for three separate experimental campaigns in October 2009, May of 2010 and November of 2010. Hardware refinements to the second stage have led to significant performance improvement.

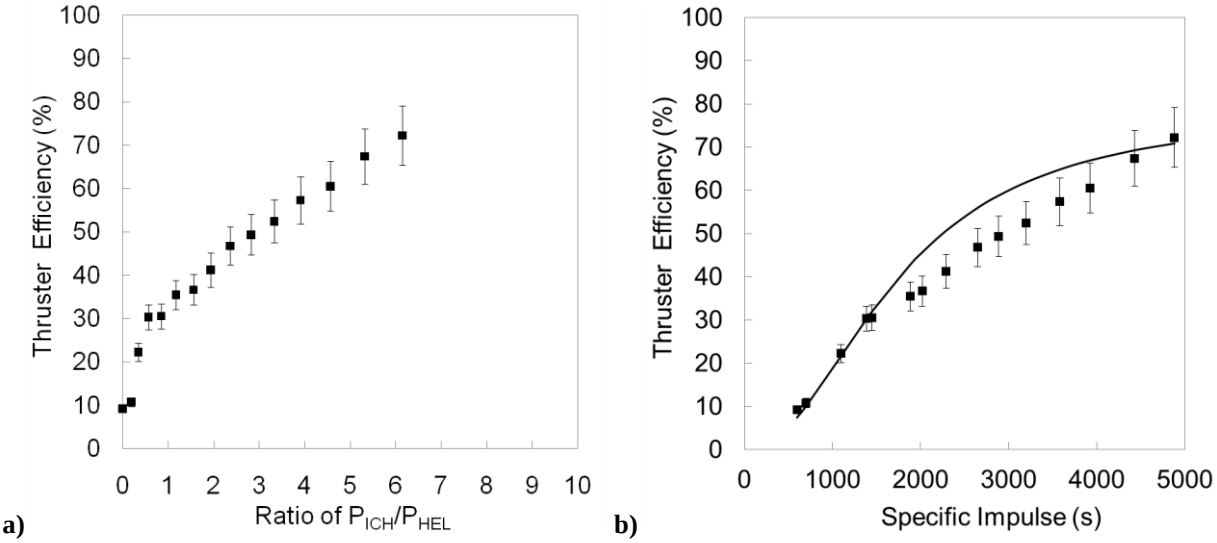

a) **b)**

Figure 10. Thruster efficiency of the VX-200 engine as a function of the ICH RF Power to Helicon RF Power, left, and as a function of specific impulse, right. A least squares fit of the data to a semi-empirical model is also superimposed, right.

The integrated current density and force density data yield a nozzle efficiency of 93% and 96% respectively. For

the following system efficiency analysis, the more conservative 93% nozzle efficiency was used. This estimate was consistent with particle trajectory modeling[72] that predicted a nozzle efficiency of 90%. Calculations based on a MHD theory[73] that factors in possible drag effects due to the plasma leaving the high magnetic strength zone yield a nozzle efficiency of 87%.

The total thruster efficiency, η_T, of the VX-200 engine was determined by dividing the total RF power coupled to the plasma by the thruster jet power, where the jet power is defined as

$$P_{jet} = \frac{F^2}{2\dot{m}} \tag{4}$$

where F is the total force produced by the rocket and $\dot{m}$ is the total mass flow rate of propellant. Dividing equation 4, by the total RF power coupled to the plasma yields

$$\eta_T = \frac{P_{jet}}{P_{1,RF}+P_{2,RF}} \tag{5}$$

where $P_{1,RF}$ and $P_{2,RF}$ represent the RF power coupled to the helicon and ICH stages of VX-200 engine respectively.

Figures 9 and 10 show the total thruster efficiency as a function of the specific impulse where the specific impulse was calculated using Eqn. 6 with measured values of force (Fig. 8) and propellant flow rate, and the total thruster efficiency was calculated using Eqn. 5. For data presented in Fig. 10, the VX-200 engine used a propellant flow rate of 107 mg/s, a helicon coupled RF power level of 29 kW, and an ICH coupled RF power level from 0 to 172 kW, which yielded results that show a total force of up to 5.8±0.4 N, at an I_{sp} of 4900±300 s, and a 72±9% thruster efficiency. Previous RPA data was used to corroborate the PMFS measurements. RPA measurements were taken at power levels up to 136 kW and matched the PMFS measurements with an error of less than 3%. At RF power levels up to 136 kW, the RPA was used to verify the PMFS results and reported a mean ion flow velocity of 32.8 km/s with an ion temperature of 24 eV in the frame of reference moving with the beam. RPA measurements were not possible at power levels higher than 136 kW as the power density of the plasma exhaust led to RPA grid degradation. However, RPA measurements showed at most a 3% error compared to the PMFS at a total RF power level of 136 kW.

$$I_{SP} = \frac{F}{\dot{m}g} \tag{6}$$

The Helicon stage was operated at a constant 28 kW coupled RF power; while the ICH stage coupled RF power was varied from 0 to 183 kW, Fig. 8. Any change to the thruster efficiency was due largely to the increasing component of ICH coupled RF power. The limiting factor in the maximum ICH coupled RF power to the VX-200 engine was a vacuum pressure limit within the vacuum chamber, where greater RF circuit voltages produced glow or arc discharges that prompted the VX-200 engine solid state RF generators to shut down. The total thruster efficiency in Figs. 9 and 10 increases as a function of coupled ICH RF power and I_{sp}, indicating that the process of ICH wave coupling into the plasma column has not saturated.

Measurements of the ionization cost, defined as the ratio of the coupled RF power to the total ion current that is extracted from the system in the exhaust section, were taken during helicon-only operation as a function of both coupled RF power and argon propellant flow rate, from 15 kW to 35 kW and 50 mg/s to 160 mg/s respectively for argon and 100 to 250 mg/s for krypton. The lowest ionization cost measurement of 80±9 eV for argon and 70±9 eV for krypton occurred with VX-200 engine settings of 33 kW coupled RF power and 160 mg/s and 18 kW coupled RF power and 160 mg/s respectively. The ionization cost term, E_i, appears in Eqn 5. Though a small fraction of ICH power may be absorbed by electrons, for the purposes of the semi-empirical model in Eqn 5, it is assumed that the ICH process does not affect E_i.

A semi-empirical model of the thruster efficiency[80,74,75] for VX-200 engine, Eqn. 7, is also shown in Figs. 9 and 10, and is a least squares fit to the data using the ICH coupling efficiency as the only free parameter, such that

$$\eta_T = \frac{\frac{1}{2}m_{Ar}g^2I_{SP}^2}{eE_i+eE_1\left(1-\frac{1}{\eta_B}\right)+\frac{\frac{1}{2}m_{Ar}g^2I_{SP}^2}{\eta_B\eta_n}} \tag{7}$$

where m_{Ar} is the atomic mass of argon, g is the gravitational acceleration, I_{SP} is the specific impulse, e is the electron charge, E_i is the ionization cost of the propellant, E_1 is the first stage (helicon) RF power coupled to the

Downloaded by University of Michigan - Duderstadt Center on December 13, 2017 | http://arc.aiaa.org | DOI: 10.2514/6.2014-4344

plasma that is converted into directed ion kinetic energy through ambipolar acceleration, η_B is the ICH efficiency, and η_n is the nozzle efficiency. The ionization cost of the propellant for 29 kW helicon power and 107 mg/s Ar was E_i=105±9 eV/ion-extracted, the kinetic energy of ions leaving the first stage was E_1=22±2 eV, and the nozzle efficiency was η_n=93%. The only free parameter is the ICH coupling efficiency, η_B, which was fit to the data using a least squares algorithm, and was found to be 89%. It should be noted that η_B also includes the efficiency loss due to the ion energy spread in the exhaust, i.e. the frozen flow losses due to the finite ion temperature. Decreasing E_i or increasing E_1 shifts the semi-empirical model curve to the left and increasing η_B or η_N shifts the curve upward. The VX-200 engine helicon and ICH couplers were designed to produce a thruster efficiency of 60% at 5000 s using 200 kW DC input power (equivalent to 186 kW of coupled helicon and ICH RF power). The measured performance of the VX-200 using the full 200 kW of RF power revealed a 72% thruster efficiency at a specific impulse of 4900±300 s, significantly exceeding the performance and design specifications. These engine performance data tell us that a high power system with VX-200 performance is capable of significant reduction in the transit time for outer planet nissions.

IV. The Jupiter Catapult Mission

The recent discovery of geysers on Europa has resulted in a renewed interest in a Europa orbiter mission. A number of strawman proposals have recently been floated to develop mission concepts that meet the scientific goals of determining the nature of the liquid water distribution inside Europa and perhaps get some indication of the chemical content of the ocean water. Sending a payload to Jupiter directly from the surface of the Earth with a single launch vehicle has always been challenging proposition. The typical transfer orbit involves multiple gravity slingshot Earth and Venus flybys in order to gain enough energy to get to Jupiter and can take upwards of 6 years. Solar electric propulsion spacecraft have never been seriously considered because the required high powered electric propulsion engines have not existed and the inverse square law limits the region where electric propulsion is practical to the region inside the orbit of Mars. The VASIMR® engine is the required high power system. This paper will present a mission profile called the ejector or catapult plan that works by generating most of the energy required when close to the Sun. A brief study of possible mission parameters will be presented.

A. The VASIMR® Ejector Catapult

The VASIMR® ejector catapult takes advantage of the inverse square law increase in solar radiation when approaching the Sun to gain the energy needed to put a payload on a direct Hohmann-like Jupiter transfer orbit. The mission plan has three phases. In phase 1, the spacecraft decelerates for a close solar pass by thrusting anti-parallel to the heliocentric velocity of the vehicle (Figure

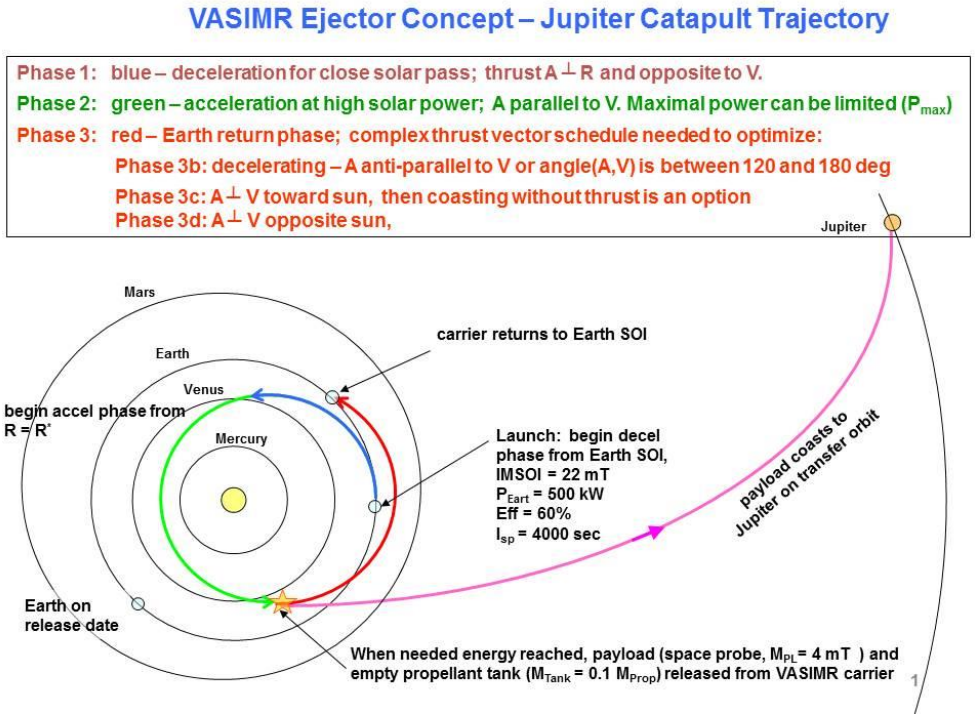

Figure 11. The interplanetary trajectory of the VASIMR® ejector concept.

Downloaded by University of Michigan - Duderstadt Center on December 13, 2017 | http://arc.aiaa.org | DOI: 10.2514/6.2014-4344

11). In phase 2, the spacecraft accelerates at high solar power, exploiting the increasing solar energy flux. The thrust is parallel to the velocity vector. The spacecraft's trajectory will pass within the orbit of Venus to a perihelion distance of ~0.54 AU. Phase 3 begins at about 0.73 AU. In the concept studies done so far, the payload now has sufficient energy to coast to Jupiter, arriving in about 3 years. The concept plan then returns the carrier spacecraft to Earth. This plan has the disadvantage of requiring more return fuel mass than the payload mass. Alternatively, the VASIMR could continue to provide thrust all the way to Jupiter. This concept has yet to be worked out in detail.

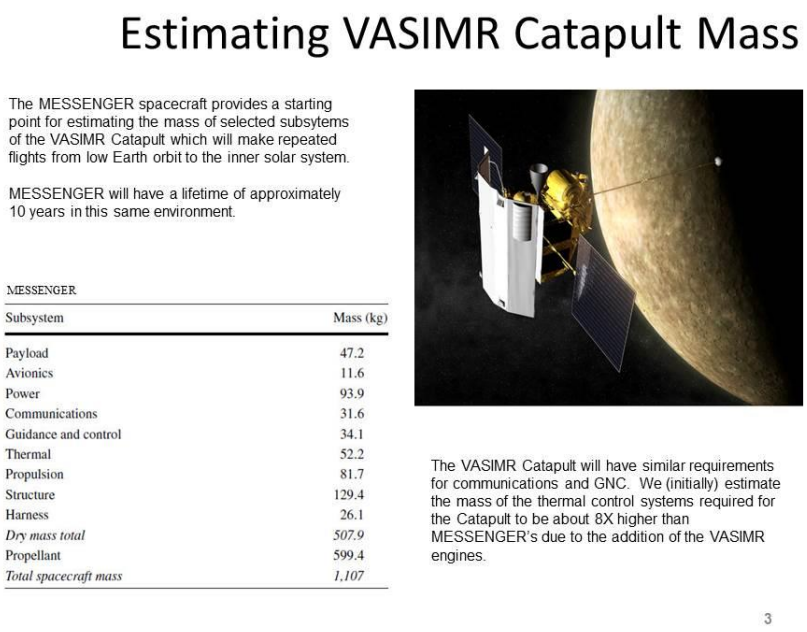

Figure 12. The masses of the MESSENGER spacecraft subsystems used as the starting point for the Catapult mass analysis

B. VASIMR Catapult Mass

The mass of the VASIMR catapult system has been estimated using the Messenger spacecraft as a template, as shown in Figure 12. Two major changes were made to the Messenger design. The thermal control systems were estimated to be a factor of eight larger than on Messenger and the propellant mass and associated tankage were increased by more than an order of magnitude.

The resulting system mass estimates are shown in Figure 13. The masses assume that the Catapult is being reused and the new propellant load and the payload are being separately delivered to LEO. The full system will have a ~22-25 mT wet mass in LEO.

C. Hohmann-like Transfer Orbit

For an initial study, it was assumed that the Catapult would release the probe as soon as the instantaneous aphelion distance intersected Jupiter's orbit (Figure 14). The study began by looking for a single trajectory that works. The solutions found specify the following

- power level
- propellant mass
- total mass of VASIMR Catapult
- payload mass
- duration of the deceleration phase
- duration of the acceleration phase
- time for the Catapult to return to Earth after releasing the payload spacecraft
- thrust vector schedule for the Earth return phase

Once this first solution was found, we varied the parameters to search for better performance, i.e., finding the lowest power level and propellant mass needed to achieve the mission. We did not complicate the problem by considering phasing (relative position of Earth and Jupiter at launch).

D. Mass Analysis with Catapult Return

The initial exploration of the parameter space considered a mission with an initial mass in low earth orbit (IMLEO) of 25 mT and a payload mass of 5 mT. These models produced a range of solutions that either forced the payload to be smaller than assumed or did not have enough argon left to get the Catapult back to Earth, as shown in Figure 15 and Table 1. However, the transit time was only 36 months, which is half the time required for Galileo to reach Jupiter. Further exploration of parameter space simulated missions with a 4 mT payload and a 22 mT IMLEO.

Downloaded by University of Michigan - Duderstadt Center on December 13, 2017 | http://arc.aiaa.org | DOI: 10.2514/6.2014-4344

Optimized solutions were found for this case that delivered the payload to Jupiter in 34.7 months (Figure 16). The major disadvantage of this mission is that it takes more argon to return the Catapult to Earth than it delivers payload to Jupiter (Figure 17).

E. An Alternative Idea

The optimum mission profile for the Catapult system ends the powered phase of flight at 0.73 AU with 5.2 mT of argon left in the tank. The reason for returning the Catapult to Earth is reuse the system for other deep-space planetary missions. The assumption is that there will be enough such missions over the next 20 years to justify building and operating a transport system capable of launching 10 missions. In the present funding environment, this scenario seems unlikely.

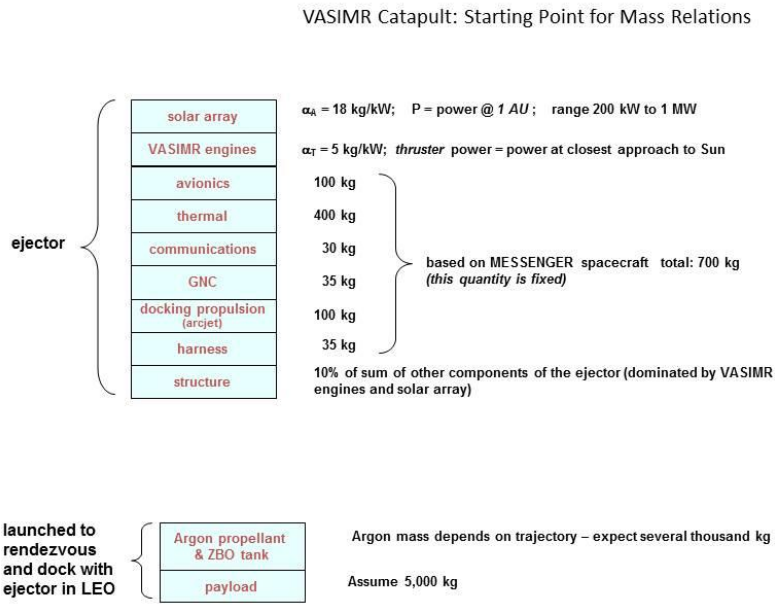

Figure 13. Initial mass estimate for catapult subsystems

One must ask, therefore, if we do not need to return the catapult system, what then could we do with it instead of detaching it. The alternative scenario has yet been studied quantitatively, but we can discuss it qualitatively. The availability of abundant solar power and reaction mass means that we are not required to turn the VASIMR off when a minimum energy Jupiter transfer orbit has been achieved. It should be possible to continue to accelerate out until at least the orbit of Mars. Deceleration into Jupiter orbit becomes trickier, since the available solar power will be down to 20 kW approaching Jupiter. Careful trade studies will have to be done, but such a mission profile may be optimized by jettisoning the argon tankage and the VASIMR magnets and thermal system at some point in mid-course and completing orbital insertion with a chemical rocket. The solar cells will still be generating 20 kW, which is abundant power for a scientific spacecraft. The RF generators can then be used as the RF sources for a radar system or topside sounder, particularly if hydrogen has been used for the cruise phase beyond 0.73 AU, which will require use of 240 MHz for the helicon frequency. Future studies will explore this concept in more detail.

V. Conclusion

The use of VASIMR® technology to provide the midcourse transfer thrust for a solar electric Jupiter mission will enable a mission to arrive in half the time required by a chemical propulsion system. It will deliver a spacecraft that is larger and more capable than the one a chemical propulsion system will deliver. If the solar arrays and VASIMR RF generators are retained for the entire mission, one will arrive with a 20 kW power system and the high power RF core of very capable ice penetrating radar.

Acknowledgments

The authors are grateful for the support of the Ad Astra Rocket Company.

Downloaded by University of Michigan - Duderstadt Center on December 13, 2017 | http://arc.aiaa.org | DOI: 10.2514/6.2014-4344

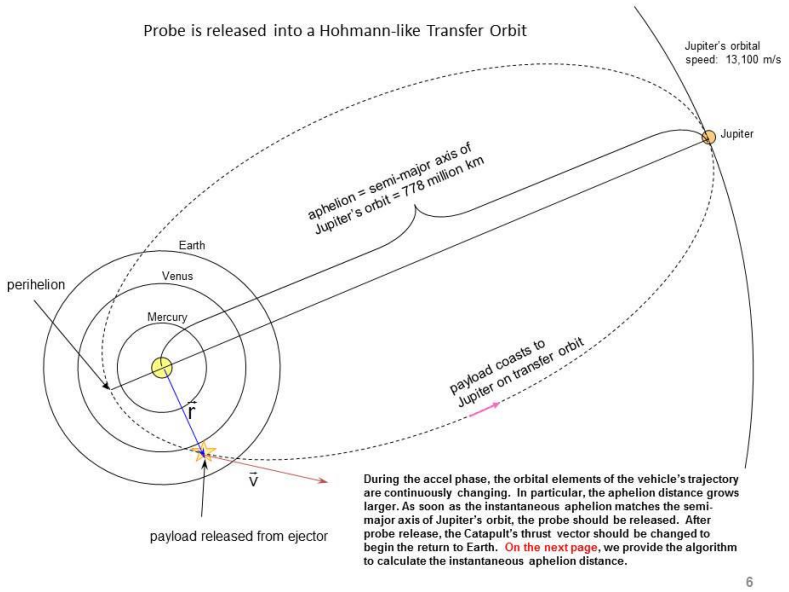

Figure 14. Hohmann-like transfer orbit injection geometry

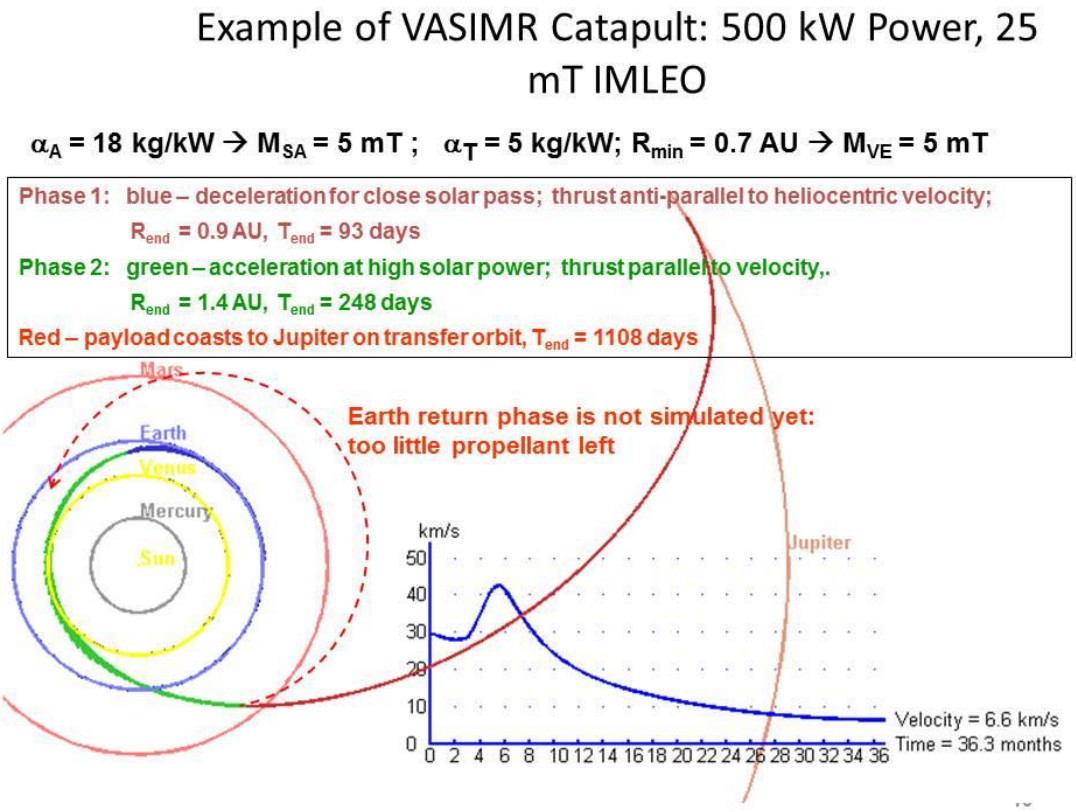

Figure 15. Optimum 25 mT IMLEO, 5mT payload model.

Downloaded by University of Michigan - Duderstadt Center on December 13, 2017 | http://arc.aiaa.org | DOI: 10.2514/6.2014-4344

Downloaded by University of Michigan - Duderstadt Center on December 13, 2017 | http://arc.aiaa.org | DOI: 10.2514/6.2014-4344

Analysis of VASIMR Catapult: 500 kW Power, 25 mT IMLEO
Thrust Reverse position was a parameter

α_A = 18 kg/kW → M_{SA} = 5 mT ; α_T = 5 kg/kW;

R_rev[AU]	0.6	0.65	0.7	0.75	0.8	0.85	0.9	0.95
R_min[AU]	0.448	0.478	0.51	0.545	0.587	0.636	0.7	0.792
R_shut[AU]	0.654	0.702	0.765	0.848	0.964	1.14	1.444	2.157
Propellant[kg]	8657	8245	7887	7569	7279	7010	6756	6527
T_shut[days]	203	203	204	207	213	224	248	323
T_jup[days]	1052	1056	1062	1068	1077	1089	1108	1147
Engine[kg]	12456	10942	9612	8417	7255	6181	5102	3986
Payload+PropLeft[kg]	-4494	-2375	-519	1146	2742	4220	5686	7166

R_{rev} = 0.9 is shown in the example at the previous slide

11

Table I. Trajectory parameters as a function of thrust reverse position.

Downloaded by University of Michigan - Duderstadt Center on December 13, 2017 | http://arc.aiaa.org | DOI: 10.2514/6.2014-4344

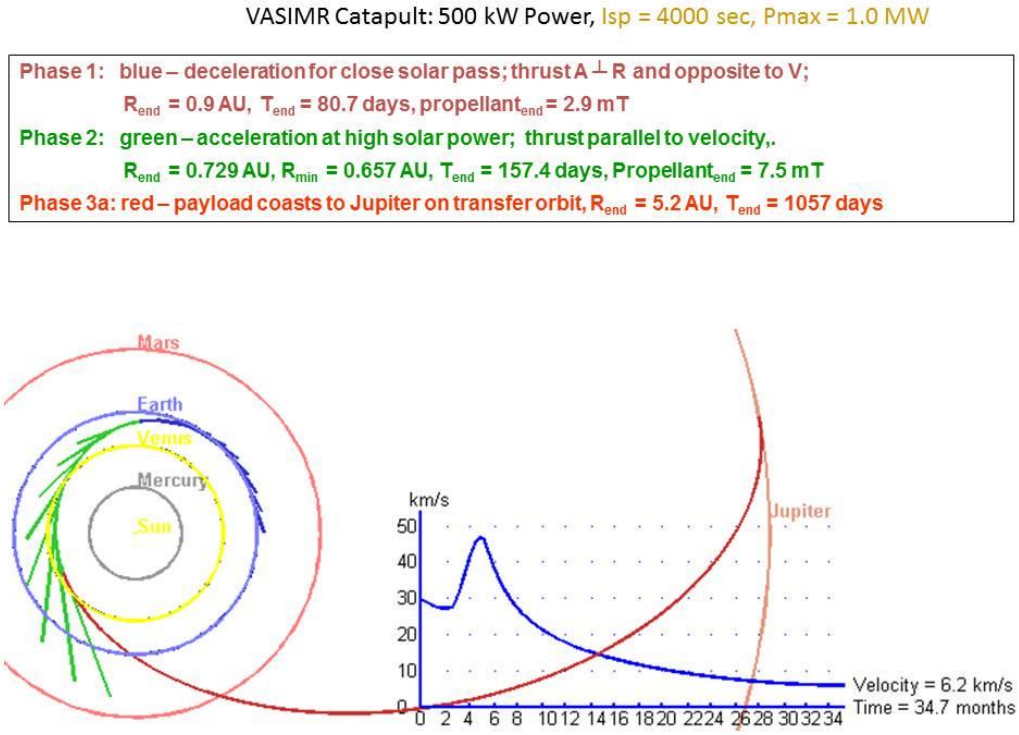

Figure 16. Model transfer orbit of a 4 mT payload, 22 mT IMLEO simulation.

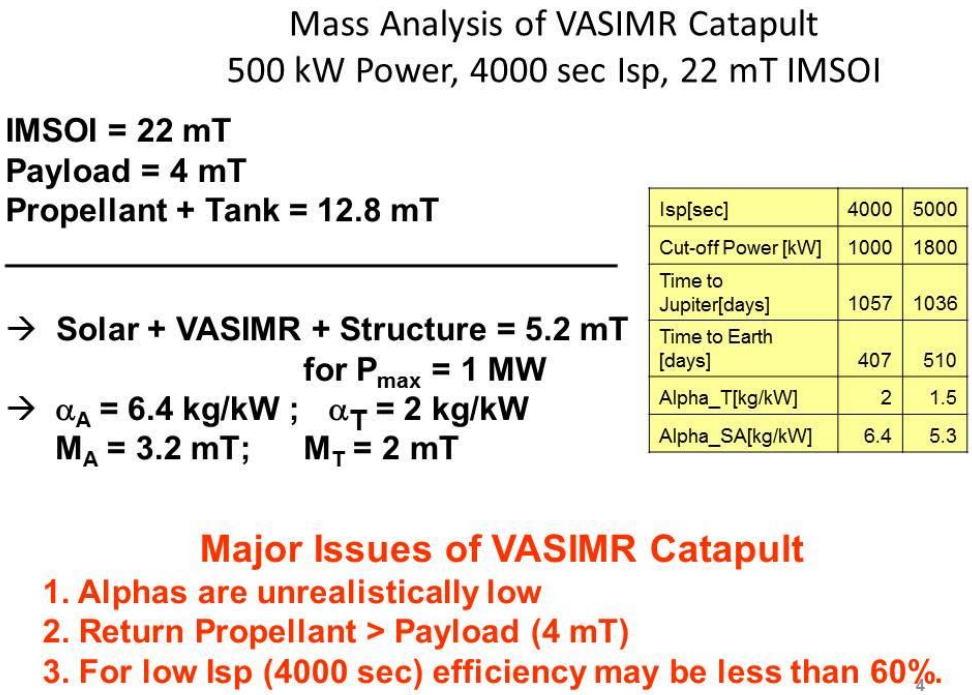

Isp[sec]	4000	5000
Cut-off Power [kW]	1000	1800
Time to Jupiter[days]	1057	1036
Time to Earth [days]	407	510
Alpha_T[kg/kW]	2	1.5
Alpha_SA[kg/kW]	6.4	5.3

Figure 17. Mass analysis of 4mT payload, 22 mT IMLEO simulation

Downloaded by University of Michigan - Duderstadt Center on December 13, 2017 | http://arc.aiaa.org | DOI: 10.2514/6.2014-4344

References

[1] K. Sankaran, L. Cassady, A. D. Kodys et al., "A survey of propulsion options for cargo and piloted missions to Mars." Presented at the *International Conference on New Trends in Astrodynamics*, Jan. 20-22, 2003 (unpublished).

[2] F. R. Chang-Díaz, "Fast, power-rich space transportation, key to human space exploration and survival." Presented at the *53rd International Astronautical Congress / The World Space Congress,* 10-19 Oct 2002, Houston, Texas, 2002.

[3] E. A. Bering III, F. R. Chang-Díaz, and J. P. Squire, "Use of RF waves in space propulsion systems, The" *Bulletin of Radio Science (310),* 92-106 (2004).

[4] R. Frisbee, "SP-100 Nuclear Electric Propulsion for Mars Cargo Missions," *29th AIAA/SAE/ASME/ASEE Joint Propulsion Conference*, Monterey, CA, USA, June 1993, AIAA-93-2092.

[5] R. Frisbee, "Electric Propulsion Options for Mars Cargo Missions," *32nd AIAA/ASME/SAE/ASEE Joint Propulsion Conference and Exhibit,* Lake Buena Vista, FL, USA, July 1996, AIAA-96-3173.

[6] A. Ilin, Cassady, L., Glover, T., Carter, M., and Chang Díaz , F., "A Survey of Missions using VASIMR for Flexible Space Exploration," Tech. Rep. JSC-65825, NASA - JSC, April 2010.

[7] R. W. Boswell and F. F. Chen, "Helicons - The early years." *IEEE Transactions on Plasma Science, 25*(6), 1229-1244 (1997).

[8] F. F. Chen and R. W. Boswell, "Helicons - The past decade." *IEEE Transactions on Plasma Science, 25*(6), 1245-12457(1997).

[9] T. G. Northrop, "The Adiabatic Motion of Charged Particles," *American Journal of Physics, Volume 32,* Issue 10, pp. 807-807 (1964).

[10] J. G. Roederer., *"Dynamics of geomagnetically trapped radiation,"* Physics and Chemistry in Space, Berlin: Springer, 1970.

[11] E. A. Bering III, Chang Díaz,F.R., Squire,J.P., Glover, T.W., Carter, M.D., McCaskill, G.E., Longmier, B.W., Brukardt, M.S., Chancery, W.J., Jacobson, V.T., "Observations of single-pass ion cyclotron heating in a trans-sonic flowing plasma," *Physics of Plasmas 17,* 043509, 2010.

[12] F. R. Chang-Díaz and J. L. Fisher, "A supersonic gas target for a bundle divertor plasma." *Nuclear Fusion 22*(8), 1982.

[13] F. R. Chang Díaz, "Research status of the Variable Specific Impulse Magnetoplasma Rocket," presented at the *39th Annual Meeting of the Division of Plasma Physics,* 1997 (unpublished).

[14] F. R. Chang Díaz, "Research Status of the Variable Specific Impulse Magnetoplasma Rocket," presented at the *Open Systems*, July 27-31, 1998, Novosibirsk, Russia, 1998 (unpublished).

[15] F. R. Chang Díaz, J. P. Squire, A. V. Ilin et al., "Development of the VASIMR™ Engine, The," presented at the *International Conference of Electromagnetics in Advanced Space Applications*, Sep 13-17, 1999, Torino, Italy, 1999 (unpublished).

[16] F. R. Chang Díaz, J. P. Squire, E. A. Bering III et al., "VASIMR™ Engine Approach to Solar System Exploration, The," presented at the *39th AIAA Aerospace Sciences Meeting and Exhibit,* Jan. 8-11, 2001, Reno, NV, 2001.

[17] F. R. Chang Díaz, J. P. Squire, T. Glover et al., "VASIMR™ Engine: Project Status and Recent Accomplishments, The," presented at the *42nd AIAA Aerospace Sciences Meeting and Exhibit,* Reno, NV, 2004.

[18] N. J. Fisch, "Confining a tokamak plasma with rf-driven currents," *Physical Review Letters, 41*(13), 873 (1978).

[19] S. N. Golovato, K. Brau, J. Casey et al., "Plasma Production and Heating in a tandem mirror central cell by radio frequency waves in the ion cyclotron frequency range," *Phys. Fluids, 3* (12), 3744-3753 (1988).

[20] Y. Yasaka, R. Majeski, J. Browning et al., "ICRF heating with mode control provided by a rotating field coupler," *Nuclear Fusion, 28,* 1765 (1988).

[21] D.G. Swanson, *Plasma Waves* (Academic Press, Boston, 1989).

[22] T. H. Stix, *Waves in Plasma* (American Institute of Physics, New York, NY, 1992).

[23] E. A. Bering III, M. Brukardt, F. R. Chang-Díaz et al., "Experimental studies of the exhaust plasma of the VASIMR™ engine." Presented at the *40th AIAA Aerospace Sciences Meeting and Exhibit,* Reno, NV, 2002.

[24] E. A. Bering III, M. S. Brukardt, W. A. Rodriguez et al., "Ion Dynamics and ICH Heating in the Exhaust Plasma of The VASIMR™ Engine." Presented at the *53rd International Astronautical Congress / The World Space Congress,* 10-19 Oct., Houston, Texas, 2002.

[25] D. G. Chavers and F. R. Chang-Díaz, "Momentum flux measuring instrument for neutral and charged particle flows." *Rev. Sci. Instrum., 73*(10), 3500-3507 (2002).

[26] B. N. Breizman and A. V. Arefiev, "Single-Pass Ion Cyclotron Resonance Absorption." *Physics of Plasmas, 8*(3), 907-915 (2001).

[27] E. G. Shelley, R. D. Sharp, and R. G. Johnson, "Satellite observations of an ion acceleration mechanism." *Geophysical Research Letters, 3*(11), 654 (1976).

[28] R. D. Sharp, R. G. Johnson, and E. G. Shelley, "Observation of an ionospheric acceleration mechanism producing energetic (keV) ions primarily normal to the geomagnetic field direction." *Journal of Geophysical Research, 82,* 3324 (1977).

[29] F. S. Mozer, C. W. Carlson, M. K. Hudson et al., "Observations of paired electrostatic shocks in the polar shocks in the polar magnetosphere." *Physical Review Letters, 38,* 292 (1977).

Downloaded by University of Michigan - Duderstadt Center on December 13, 2017 | http://arc.aiaa.org | DOI: 10.2514/6.2014-4344

[30] A. G. Ghielmetti, R. G. Johnson, R. D. Sharp et al., "The latitudinal, diurnal and altitudinal distributions of upward flowing energetic ions of ionospheric origin." *Geophysical Research Letters, 5,* 59 (1978).

[31] E. G. Shelley, "Heavy ions in the magnetosphere." *Space Science Reviews, 23,* 465 (1979).

[32] R. D. Sharp, R. G. Johnson, and E. G. Shelley, "Energetic particle measurements from within ionospheric structures responsible for auroral acceleration processes." *Journal of Geophysical Research, 84,* 480 (1979).

[33] H. L. Collin, R. D. Sharp, E. G. Shelley et al., "Some general characteristics of upflowing ion beams over the auroral zone and their relationship to auroral electrons." *Journal of Geophysical Research, 86,* 6820 (1981).

[34] M. Zintl, R. McWilliams, and N. Wolf, "Transverse ion acceleration and ion conic formation in a divergent-field laboratory plasma." *Physics of Plasmas, 2* (12), 4432-4441 (1995).

[35] M. André, P. Norqvist, L. Andersson, L. Eliasson, A.L. Eriksson, L. Blomberg, R. Erlandson, and J. Waldemark, "Ion energization mechanisms at 1700 in the auroral region." *Journal of Geophysical Research, 103* (A3), 4199-4222 (1998).

[36] J. M. Kindel, and C.F. Kennel, "Topside current instabilities." *Journal of Geophysical Research, 76,* 3055 (1971).

[37] E. Ungstrup, D.M. Klumpar, and W.J. Heikilla, "Heating of ions to superthermal energies in the topside ionosphere by electrostatic ion cyclotron waves." *Journal of Geophysical Research, 84,* 4289 (1979).

[38] M. Ashour-Abdalla, H. Okuda, and C. Cheng, "Acceleration of heavy ions on auroral field lines." *Geophysical Research Letters, 8,* 795-798 (1981).

[39] T. Chang, G.B. Crew, N. Hershkowitz, J.R. Jasperse, J.M. Retterer, and J.D. Winningham, "Transverse acceleration of oxygen ions by electromagnetic ion cyclotron resonance with broad band left-hand polarized waves." *Geophysical Research Letters, 13* (7), 636-639 (1986).

[40] R. E. Erlandson, L.J. Zanetti, T.A. Potemra, M. André, and L. Matson, "Observation of electromagnetic ion cyclotron waves and hot plasma in the polar cusp." *Geophysical Research Letters, 15,* 421 (1988).

[41] R. E. Erlandson, L.J. Zanetti, M.H. Acuna, A.I. Eriksson, L. Eliasson, M. Boehm, and L.G. Blomberg, "Freja observations of electromagnetic ion cyclotron ELF waves and transverse oxygen ion acceleration on auroral field lines." *Geophysical Research Letters, 21* (17), 1855-1858 (1994).

[42] J. E. Borovsky, "The production of ion conics by oblique double layers." *Journal of Geophysical Research, 89* (A4), 2251-2266 (1984).

[43] R. McWilliams, and R. Koslover, "Laboratory observation of ion conics by velocity space tomography of a plasma." *Physical Review Letters, 58* (1), 37-40 (1987).

[44] E. A. Bering III, M. C. Kelley, and F. S. Mozer, "Observations of an intense field aligned thermal ion flow and associated intense narrow band electric field oscillations." *Journal of Geophysical Research, 80* (34), 4612-4620 (1975).

[45] E. A. Bering III and M. C. Kelley, "Observation of Electrostatic Ion Cyclotron Waves at the Boundary of an Auroral Arc." *EOS, Transactions, American Geophysical Union, 56,* 173 (1975).

[46] M. C. Kelley, E. A. Bering III, and F. S. Mozer, "Evidence that the electrostatic ion cyclotron instability is saturated by ion heating." *Physics of Fluids, 18,* 1590-1597 (1975).

[47] P. M. Kintner, M. C. Kelley, and F. S. Mozer, "Electrostatic hydrogen cyclotron waves near one earth radius altitude in the polar magnetosphere." *Geophysical Research Letters, 5,* 139 (1978).

[48] P. M. Kintner, M. C. Kelley, R. D. Sharp et al., "Simultaneous observations of energetic (keV) upstreaming ions and electrostatic hydrogen cyclotron waves." *Journal of Geophysical Research, 84,* 7201-7212 (1979).

[49] P. M. Kintner, "On the distinction between electrostatic ion cyclotron waves and ion cyclotron harmonic waves." *Geophysical Research Letters, 7,* 585 (1980).

[50] E. A. Bering III, "Apparent Electrostatic Ion Cyclotron Waves in the Diffuse Aurora." *Geophysical Research Letters, 10,* 647-650 (1983).

[51] E. A. Bering III, "The Plasma Wave Environment of an Auroral Arc, 1., Electrostatic Ion Cyclotron Waves in the Diffuse Aurora." *Journal of Geophysical Research, 89,* 1635-1649 (1984).

[52] P. M. Kintner, W. Scales, J. Vago et al., "Harmonic H^+ gyrofequency structures in auroral hiss observed by high-altitude auroral sounding rockets." *Journal of Geophysical Research, 96*(A6), 9627-9638 (1991).

[53] J. Bonnell, P. Kintner, J.E. Wahlund, K. Lynch, and R. Arnoldy, "Interferometric determination of broadband ELF wave phase velocity with a region of transverse auroral ion acceleration." *Geophysical Research Letters, 23* (23), 3297-3300 (1996).

[54] P. M. Kintner, J. Bonnell, R. Arnoldy, K. Lynch, C. Pollock, and T. Moore, "SCIFER – Transverse ion acceleration and plasma waves." *Geophysical Research Letters, 23,* 1873-1876 (1996).

[55] P. M. Kintner, P.W. Schuck, and J.R. Franz, "Spaced measurements and progress in understanding space plasma waves." *Physics of Plasmas, 7* (5), 2135-2141 (2000a).

[56] P. M. Kintner, J. Franz, P. Schuck, and E. Klatt, "Interferometric coherency determination of wavelength or what are broadband ELF waves?" *Journal of Geophysical Research, 105* (A9), 21237-21250 (2000b).

[57] W. E. Amatucci, D.N. Walker, G. Ganguli, D. Duncan, J. Antoniades, J.H. Bowles, V. Gavrishchaka, and M.E. Koepke, "Velocity-shear-driven ion-cyclotron waves and associated transverse ion heating." *Journal of Geophysical Research, 103* (A6), 11711-11724 (1998).

[58] D. L. Correll, H. Boehmer, N. Rynn, and R.A. Stern, "Temporal evolution of ion temperatures in the presence of ion cyclotron instabilities." *Physics of Fluids, 20* (5), 822-828 (1976).

[59] S. Cartier, N. D'Angelo, and R. Merlino, "A laboratory study of ion energization by EIC waves and subsequent upstreaming along diverging magnetic field line." *Journal of Geophysical Research, 91* (A7), 8025-8033 (1986).

[60] A. Fruchtman, "Double layer and thrust." *47th Annual Meeting of the Division of Plasma Physics, Bulletin of the American Physical Society, 50,* pp. 109, Denver, Colorado. (2005).

[61] J. P. Squire, F. R. Chang-Díaz, V. T. Jacobson et al., "Helicon plasma injector and ion cyclotron acceleration development in the VASIMR™ experiment." Presented at the *36th AIAA/ASME/SAE/ASEE Joint Propulsion Conference*, July 17-19, Huntsville, Alabama, 2000.

[62] A. Petro, F. R. Chang-Díaz, A. V. Ilin et al., "Development of a space station-based flight experiment for the VASIMR™ magneto-plasma rocket." Presented at the *40th AIAA Aerospace Sciences Meeting and Exhibit*, 14-17 January, Reno, NV, 2002.

[63] F. R. Chang Díaz, "An overview of the VASIMR™ engine: High power space propulsion with RF plasma generation and heating." Presented at the *14th Topical Conference on Radio Frequency Power in Plasmas*, May 7-9, Oxnard, CA, 2001 (unpublished).

[64] R. W. Boswell, "Very efficient plasma generation by whistler waves near the lower hybrid frequency." *Plasma Phys. Control. Fusion, 26*, 1147 (1984).

[65] F. F. Chen, "Plasma ionization by helicon waves." *Plasma Physics and Controlled Fusion*, *33*(4), 339-364 (1991).

[66] R. W. Boswell and F. F. Chen, "Helicons - The Early Years." *IEEE Transactions on Plasma Science*, *25*(6), 1229-1244 (1997).

[67] R. W. Boswell and C. Charles, "The helicon double layer thruster." Presented at the *28th International Electric Propulsion Conference, IEPC 2003,* Toulouse, France, 2003.

[68] B. W. Longmier, J.P.Squire, C. S. Olsen, L. D. Cassady, M. G. Ballenger, M. D. Carter, A. V. Ilin, T. W. Glover, G. E. McCaskill, F. R. Chang Diaz, and E. A. Bering III, *Improved Efficiency and Throttling Range of the VX-200 Magnetoplasma Thruster.* Journal of Propulsion and Power, 2013.

[69] L. D. Cassady, Longmier, B.W., Olsen, C.S., Ballenger, M.G., McCaskill, G.E., Ilin, A.V., Carter, M.D., Glover, T.W., Squire, J.P. , Chang Díaz, F.R., "VASIMR Performance Results," AIAA Paper 2010-6772, *46th AIAA/ASME/SAE/ASEE Joint Propulsion Conference & Exhibit*, Nashville, TN, 25-28 July, 2010.

[70] W. Cox, C. Charles,R. Boswell, and R. Hawkins, Spatial retarding field energy analyzer measurements downstream of a helicon double layer plasma, *Appl. Phys. Lett., 93,* 071505 2008.

[71] G. Sutton and O. Biblarz, *Rocket Propulsion Elements*, 7th edition, John Wiley & Sons, Inc., 2001.

[72] Ilin, A., Chang Díaz , F., Squire, J., Tarditi, A., Breizman, B., and Carter, M., "Simulations of Plasma Detachment in VASIMR," *40th AIAA Aerospace Sciences Meeting and Exhibit* , Reno, NV, January 14-17 2002, AIAA 2002-0346.

[73]Arefiev, A. and Breizman, B., "Magnetohydrodynamic scenario of plasma detachment in a magnetic nozzle," *Physics of Plasmas, Vol. 12*, 2005

[74] H. Böhrk and M. Auweter-Kurtz, Thrust measurement of the hybrid electric thruster TIHTUS by a baffle plate, *J. Propulsion Power Vol. 25*, No. 3, pp. 729-736, 2009.

[75] B. W. Longmier , L. D. Cassady, M. G. Ballenger, M. D. Carter, F. R. Chang Díaz, T. W. Glover, A. V. Ilin, G. E McCaskill, C. S. Olsen, J. P. Squire, E. A. Bering, III, "VX-200 Magnetoplasma Thruster Performance Results Exceeding 50% Thruster Efficiency," , *J. Prop. Power, Vol. 27*, No. 4, doi:10.2514/1.B34085, 2011.

Downloaded by University of Michigan - Duderstadt Center on December 13, 2017 | http://arc.aiaa.org | DOI: 10.2514/6.2014-4344